Material Analysis of Cu End-Point Detection for Advanced Node PFIB Delayering Process Optimization

Or Haimson[1], Thibaut Dessolier[2], David Donnet[2], Zdeněk Král[2], Tzach Jaffe[1], Hagit Sagi[1]

[1] Annapurna Labs Ltd. an Amazon Company, Matam Scientific Industries Center, Building 19, Haifa 3508409, ISRAEL

[2] Thermo Fisher Scientific, Achtseweg Noord 5, 5651 GG Eindhoven, the Netherlands

Introduction

As integrated circuits continue to scale down to ever-smaller dimensions and increased complexity, traditional failure isolation & analysis (FA/FI), and sample preparation techniques face significant limitations. The increasing density of modern semiconductor devices, now advancing beyond 3 nm technology nodes, presents unprecedented challenges in precise layer-by-layer analysis. Over the past decade, Xenon (Xe) Plasma Focused Ion Beam (PFIB) gas assisted delayering has emerged as a standard industry technique for precise layer-by-layer delayering of integrated circuits.

Recent studies have validated PFIB delayering as an effective sample preparation technique for nanoprobing applications. Research on 14 nm FinFET devices in SRAM arrays has demonstrated the technique's capability to provide clean, artifact-free surfaces suitable for atomic force nanoprobing (1). Furthermore, advancements in PFIB delayering have enabled successful nanoprobing of 5 nm node devices (2), confirming its applicability to cutting-edge semiconductor technologies.

While previous studies have focused on electrical and topographical characterization of PFIB delayering (3,4), comprehensive material and chemical analysis of the delayering process remains crucial, particularly for Cu interconnect end-point monitoring. This study addresses the chemical and structural characterization of PFIB-delayered surfaces, with specific emphasis on the material properties of Cu lines end-point detection.

This comprehensive characterization aims to optimize failure analysis protocols and establish parameters for automated end-point detection.

Experimental

An advanced process node microprocessor was used for the scope of this investigation. The whole sample was mechanically de-processed to the bottom of Via 4 as a starting point, over a cache memory area of standard 6T SRAM cells. The PFIB delayering was carried out on a Thermofisher Helios 5 CXe PFIB tool.

Initially, a 20 by 20 um^2 area was delayered by using a Dx gas flow of ~10^{-5} mbar; beam energy of 5 keV and beam current equivalent to 1 nA. The PFIB beam parameters were chosen in accordance with previous studies that validate them to be suitable for device nanoprobing with minimal electrical device alteration while keeping good planarity over the region of interest (ROI) (4). The stage current was used as the endpoint monitor as it allows the progress of the delayering to be monitored and clearly distinguishes between vias and metal lines, thus making it a powerful tool for precise sample

preparation. The stage current for the delayering from via 4 down to the bulk silicon was used as a reference (Figure 1).

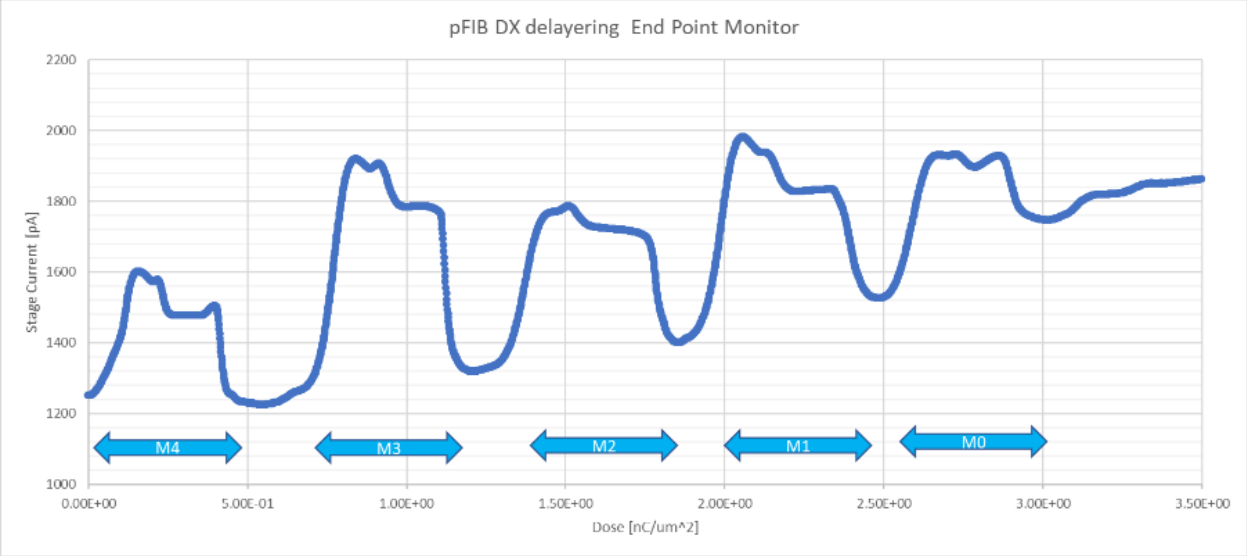

Fig.1 Stage current end point monitor over a standard memory block.

As can be noted from the stage current end point monitor, and in agreement with previous studies concerning PFIB delayering of Cu lines, these are common stage current based end point monitor plots (2,4).

In this work, we focused on the metal three layer. The metal three delayering dose is limited to the region of roughly 0.82 to 1.1 nC/um^2. Six different areas were delayered by specific dose using the mentioned parameters (Figure 2). Each site was then protected by an electron beam W deposition of ~200 nm, at the center of the processed area. An additional non-delayered site was also prepared as a reference to characterize the metal three stack and etch stop layer.

The peak stage current can be divided into two main regimes: the first at dose range of 0.81-0.91 nC/um^2 with the stage current of around 1900 picoamperes (red area on Figure 2), and the second at dose range of 0.98-1.1 nC/um^2 of around 1780 picoamperes (blue area on Figure 2).

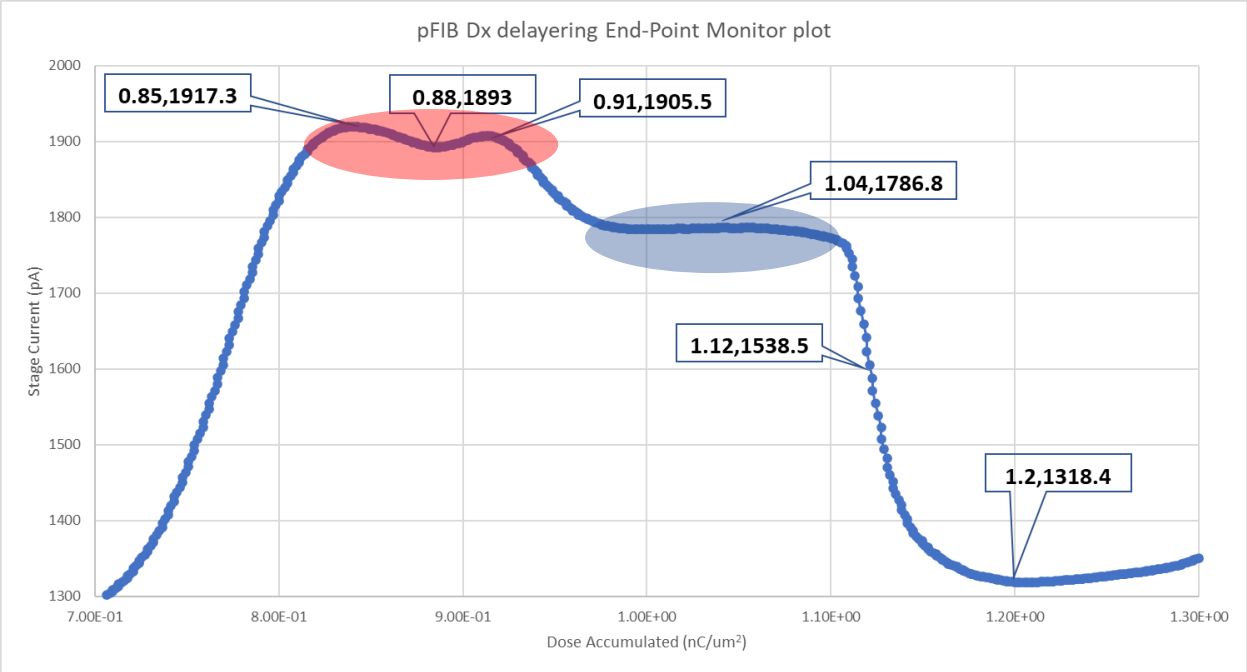

Fig.2 Metal 3 Stage current end point monitor indicating the different dose areas that were analyzed.

Planar SEM images of the whole delayered areas were taken to correlate the stage current to the uniformity of etching process.

Finally, seven cross lamellas were prepared using the Thermo Fisher AutoTEM and were analyzed using HR TEM & EDS analysis. Each lamella was taken from the center of the delayered area.

Results

STEM images of the reference area lamella (Figure 3a) clearly show the Cu metal stack over the 6T SRAM cache area. High-magnification images (Figure 3b & 3c) reveal distinct layers including Al etch stop, Co capping, and Cu metal 3 layers. The Al etch stop layer exhibits a distinctive dual-layer structure with a thick upper layer and thinner lower layer separated by silicon oxide.

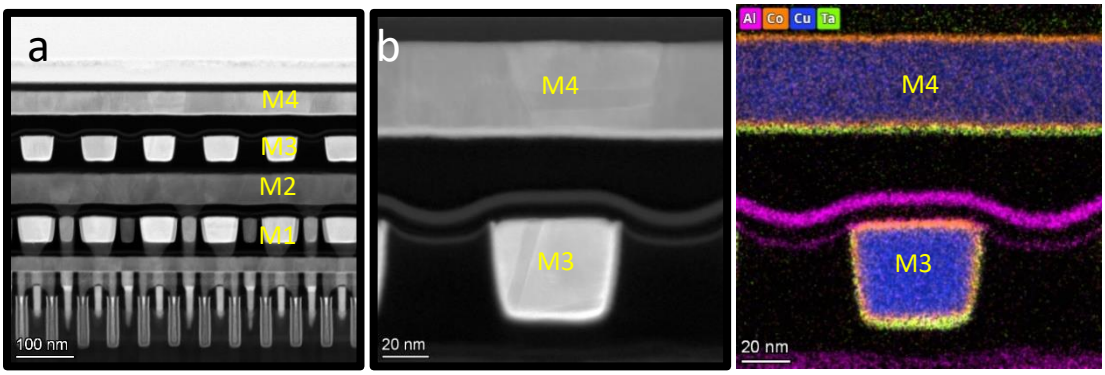

Fig.3 STEM images of reference sample. (a) Overview of the whole stack starting with metal 4 on the top down to the bulk Si on the bottom. (b) STEM high magnification and layer labeling. (c) EDS of metal 3 indicating the Al etch stop, Co capping and Cu metal layers.

The SEM, HR STEM HAADF images, and EDS analysis lamellae that were taken for each of the different PFIB Dx delayering doses are compared (Figure 4).

PFIB Dose	Planar secondary electrons 3keV SEM	HR STEM HAADF metal 3 high magnification	Metal 3 EDS elements mapping
0.85 [nC/um^2]	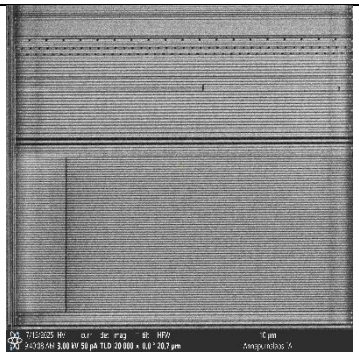	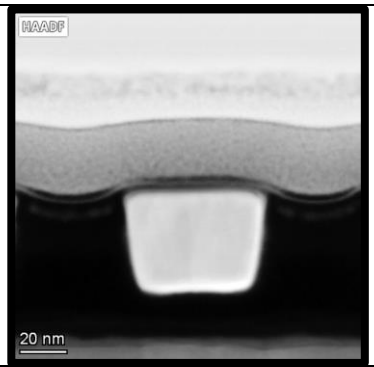	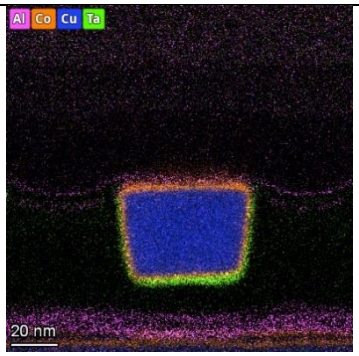
0.88 [nC/um^2]	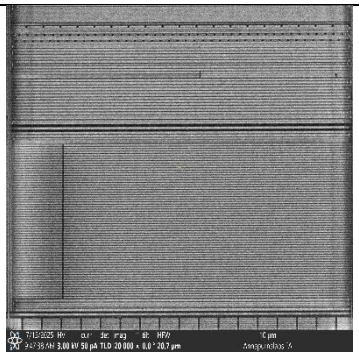	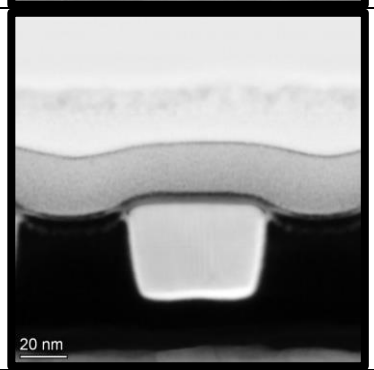	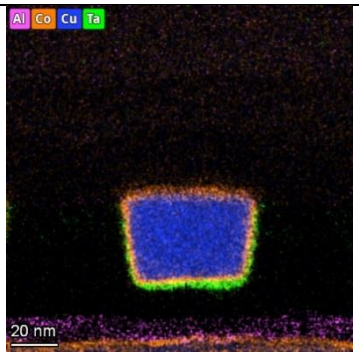
0.91 [nC/um^2]	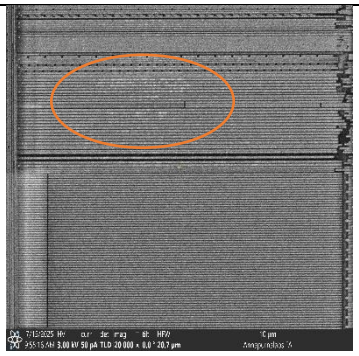	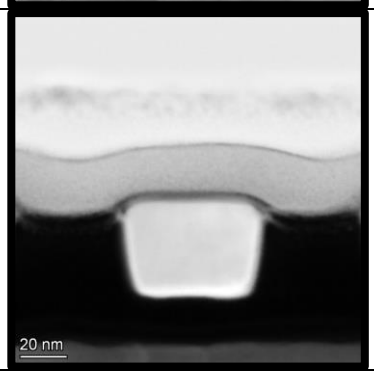	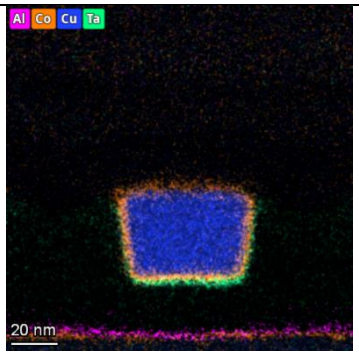

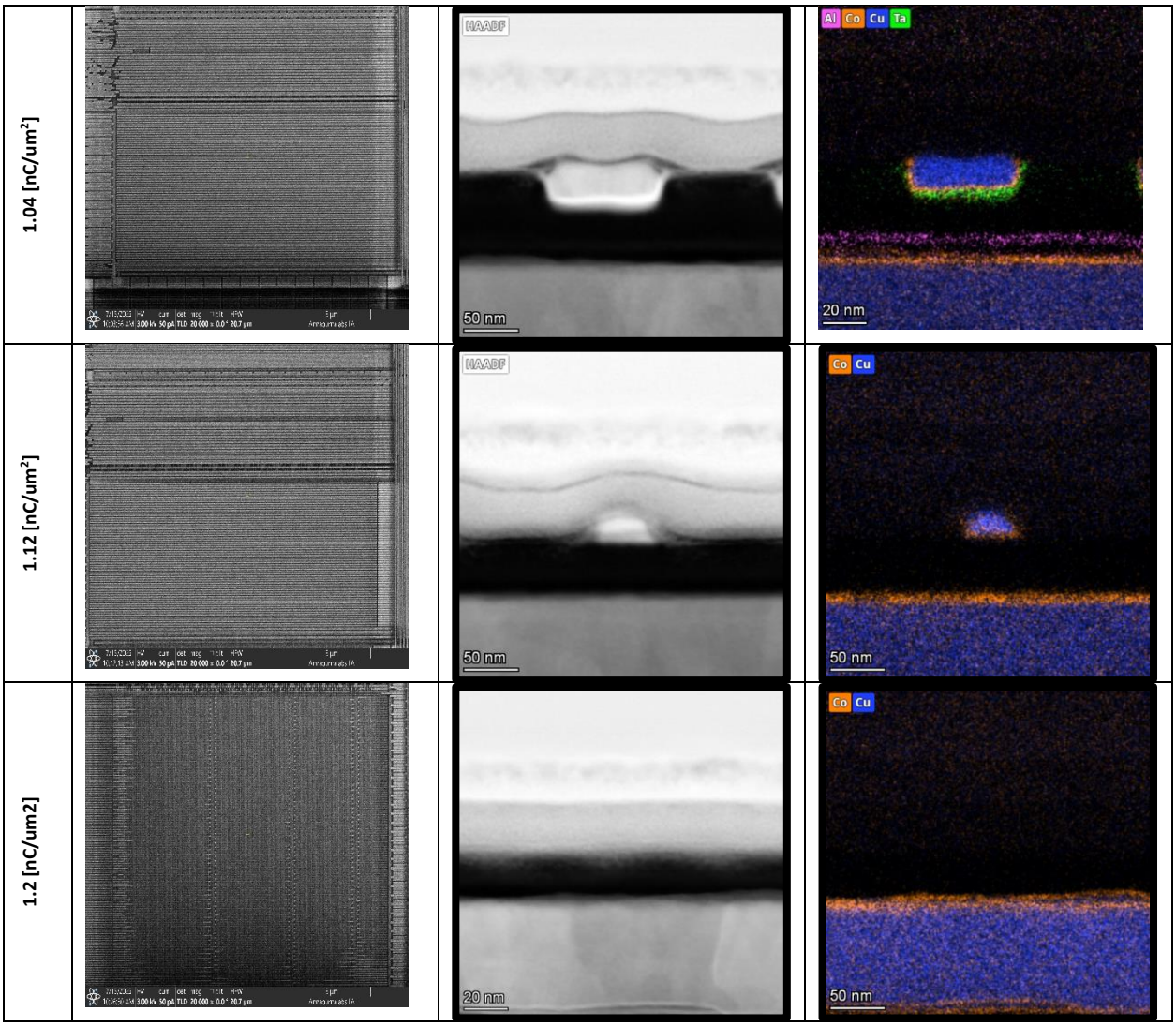

Fig.4 SEM, HR STEM & EDS Images of PFIB Dx delayered samples correlated to the beam dose.

The low PFIB Dx etching dose of 0.85 nC/um^2 indicates good uniformity across the processed area. We note that the thick Al etch stop layer was delayered, but the thin Al etch stop layer and the Co capping above the Cu metal 3 layer are intact.

Increasing the PFIB Dx etching dose to 0.88 & 0.91 nC/um^2 slightly etches the thin Al etch stop layer and starts to delayer the Co capping above the Cu metal. In addition, the planview SEM image indicates that for the higher dose of 0.91 nC/um^2, the whole processed areas starts to slightly lose uniformity and there are areas where the Cu metal 3 layer is exposed (marked in orange in Figure 4). Since the cross-section lamella was prepared at the center of each sample, this etch is not evident at the STEM & EDS.

We note that at these low doses, the stage current endpoint monitor indicates 30 picoamperes fluctuations.

With the increase of the etching dose, the Cu metal lines are clearly etched until finally removed. The planar SEM image shows the high uniformity of the PFIB Dx etching.

Discussion

The systematic analysis of PFIB delayering across multiple doses reveals critical insights into end-point detection optimization. The observed stage current variations demonstrate a strong correlation with specific layer transitions, particularly during Cu metal exposure. Most notably, the characteristic 30 picoampere fluctuations observed at doses between 0.88-0.91 nC/um^2 serve as a reliable indicator for approaching the Cu metal layer. This distinctive signal pattern provides a promising parameter for developing automated endpoint detection protocols.

Further analysis reveals that 0.91 nC/um2 represents a critical threshold dose at which the delayering process begins to expose the underlying Cu metal layer. Beyond this dose, we observe a systematic progression of Cu metal removal, ultimately achieving highly uniform delayering across the processed area at higher doses. This dose-dependent behavior suggests a two-stage approach for precise Cu layer removal: an initial careful approach to the metal layer using the characteristic current fluctuations as guidance, followed by controlled removal at higher doses to achieve uniform delayering.

Conclusion

This comprehensive material analysis of Cu end-point detection in PFIB delayering processes provides crucial insights for advanced node semiconductor failure analysis. Our systematic investigation reveals distinct correlations between delayering doses and material removal patterns. These findings establish quantitative parameters for automated endpoint detection protocols for applications such as nanoprobing (6)

The practical application of these findings is demonstrated through a case study on a logic area, where precise dose control (Figure 6) proved essential for optimal passive voltage contrast imaging.

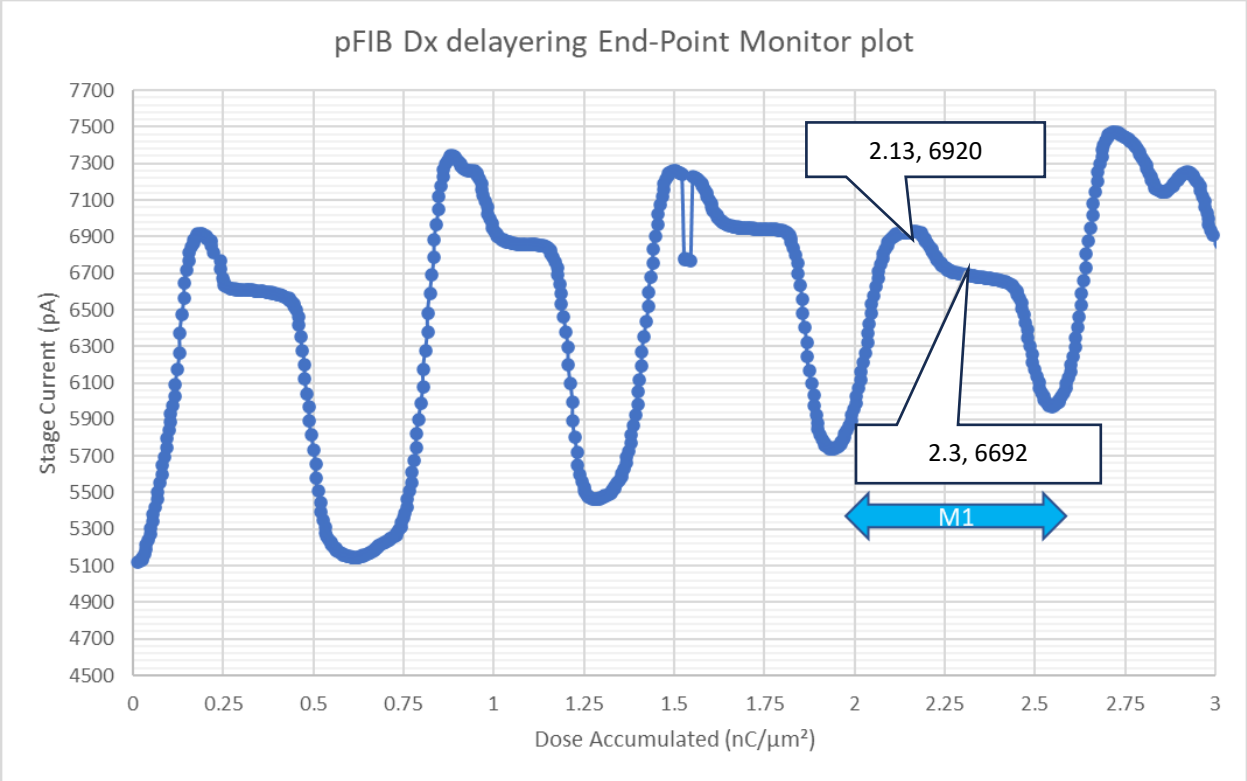

Fig.6 Stage current end point monitor over a reference logic area. The data labels indicate the ROI area patterning dose used.

Initial delayering at 2.13 nC/um^2 resulted in weak PVC signals and residual etch-stop layer material over metal lines (Figure 7a). Increasing the dose to 2.3 nC/um2 significantly improved image contrast and successfully removed residual materials (Figure 7b), highlighting the critical relationship between delayering parameters and analytical outcome quality.

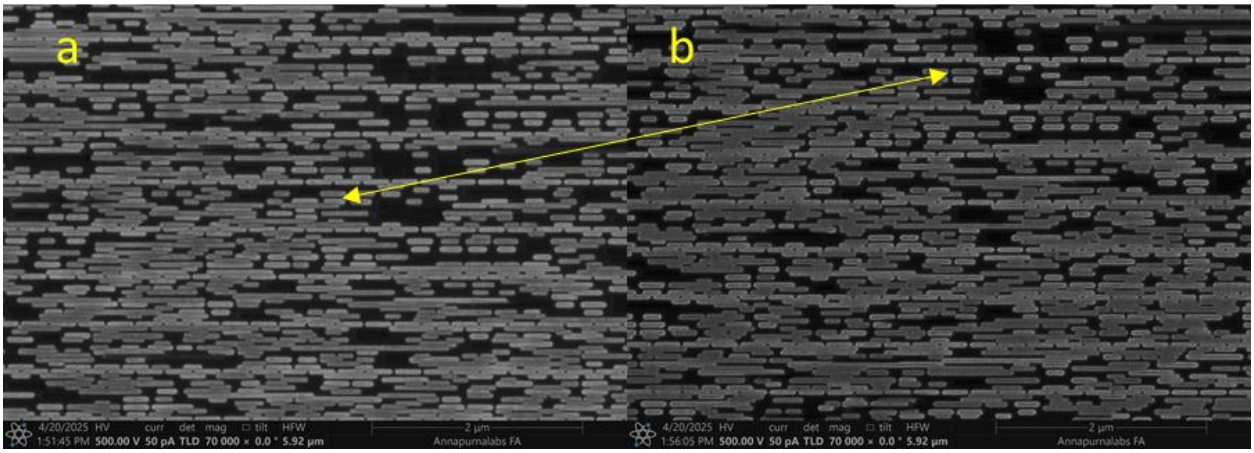

Fig.7 Low beam energy SEM PVC images of logic area. (a) Low dose PFIB delayering – weak PVC signal & residues observed on metal layer. (b) Addition PFIB delayering dose drastically improves PVC signal and removes residues.

These results establish a framework for optimizing PFIB delayering protocols, particularly for advanced node technologies where precise layer control is crucial. The combination of stage current monitoring and dose-dependent material removal characteristics provides a robust foundation for developing automated delayering processes. This approach can maintain consistency and reliability in semiconductor failure analysis applications, paving the way for more efficient and accurate diagnostics in increasingly complex integrated circuit architectures.

Acknowledgments

The authors gratefully acknowledge Chloe Minnai from Thermo Fisher Scientific Nanoport, Eindhoven, Netherlands, for conducting all TEM and EDS analyses presented in this work.

References

[1] Roger Alvis, Trevan Landin, Chad Rue, Peter Carleson, Oleg Sidorov, Andrew Erickson, Sean Zumwalt, Sinjin Dixon-Warren, Wan-Yi Liu, Shih-Hsin Chang, Te-Fu Chang, Chia-Hsiang Yen, Pau-Sheng Kuo, Chih-Hsun Chu; November 1–5, 2015. "Plasma FIB DualBeam Delayering for Atomic Force NanoProbing of 14 nm FinFET Devices in an SRAM Array." Proceedings of the *ISTFA 2015*. *ISTFA 2015: Conference Proceedings from the 41st International Symposium for Testing and Failure Analysis*. Portland, Oregon, USA. (pp. pp. 388-400). ASM. https://doi.org/10.31399/asm.cp.istfa2015p0388

[2] Ha Young Choi, Christopher H. Kang, William Lowe; October 30–November 3, 2022. "PFIB Delayering—Nanoprobing Workflow on 5nm FinFET device." Proceedings of the *ISTFA 2022*. *ISTFA 2022: Conference Proceedings from the 48th International Symposium for Testing and Failure Analysis*. Pasadena, California, USA. (pp. pp. 269-276). ASM. https://doi.org/10.31399/asm.cp.istfa2022p0269

[3] Pete Carleson, David Donnet, Oleg Sidorov, Chad Rue; November 9–13, 2014. "Delayering on Advanced Process Technologies Using FIB." Proceedings of the *ISTFA 2014*. *ISTFA 2014: Conference Proceedings from the 40th International Symposium for Testing and Failure Analysis*. Houston, Texas, USA. (pp. pp. 430-435). ASM. https://doi.org/10.31399/asm.cp.istfa2014p0430

[4] C. -C. Lin, Y. -D. Li and K. Hsu, "Guidelines of Plasma-FIB Delayering Techniques for Advanced Process Node," *2021 IEEE International Symposium on the Physical and Failure Analysis of Integrated Circuits (IPFA)*, Singapore, Singapore, 2021, pp. 1-4, doi: 10.1109/IPFA53173.2021.9617324.

[5] Micah Ledoux, James Clarke, Brett Avedisian, Chad Rue, Umesh Adiga, and Mark Biedrzycki "Gas-enhanced PFIB surface preparation enabled metrology and statistical analysis of 3D NAND devices", Proc. SPIE 10959, Metrology, Inspection, and Process Control for Microlithography XXXIII, 109590I (26 March 2019); https://doi.org/10.1117/12.2515069

[6] Branden Long, Yang Su, Yunfei Wang, Christopher Morgan, Md Faisal Kabir, Ramya Padmanaban, Weston Hearne, Tad Daniel; November 12–16, 2023. "Nanoprobing for Logical Cell Operational Tests." Proceedings of the *ISTFA 2023*. *ISTFA 2023: Conference Proceedings from the 49th International Symposium for Testing and Failure Analysis*. Phoenix, Arizona, USA. (pp. pp. 420-426). ASM. https://doi.org/10.31399/asm.cp.istfa2023p0420